Dichroism of x-ray fluorescence under standing waves regime in magnetic periodic multilayers

Philippe Jonnard, Meiyi Wu, Jean-Michel André, Karine Le Guen, Franz Schäfers, Andrey Sokolov, Elena O Filatova, Adriano Verna, Zhanshan Wang, Qiushi Huang

Dichroism of x-ray fluorescence under standing waves regime in magnetic periodic multilayers

Philippe Jonnard[1], Meiyi Wu[1], Jean-Michel André[1], Karine Le Guen[1], Franz Schäfers[2], Andrey Sokolov[2], Elena O. Filatova[3], Adriano Verna[4], Zhanshan Wang[5], Qiushi Huang[5]

[1] Sorbonne Université, Département des Sciences et Ingénierie, UMR CNRS, Laboratoire de Chimie Physique - Matière et Rayonnement, 4 place Jussieu, F-75252 Paris cedex 05, France
[2] Helmholtz-Zentrum Berlin für Materialien und Energie, BESSY-II, Albert-Einstein-Str. 15, 12489 Berlin, Germany
[3] Institute of Physics, St-Petersburg State University, Ulyanovskaya Str. 1, Peterhof, 198504 St. Petersburg, Russia
[4] Dipartimento di Scienze, Università degli Studi Roma Tre, Via della Vasca Navale 84, I-00146 Roma, Italy
[5] Key Laboratory of Advanced Micro-Structured Materials MOE, Institute of Precision Optical Engineering, School of Physics, Science and Engineering, Tongji University, Shanghai 200092, China

Keywords: dichroism, standing waves, interface, x-ray emission, fluorescence, multilayer, cobalt

Abstract

We present the first test of the implementation of a characterization method whose aim is to study the interfaces of magnetic and periodic hetero-structures. The methodology relies on the combination of two techniques, generation of x-ray standing waves and dichroism in x-ray emission. The first one gives the depth selectivity since the maximum of the electric field can be put in specific locations of the stack, the centre of layers or their interfaces, while the second one enables being sensitive to the magnetic character of the atoms present within the stack. To concentrate on the methodology, the well-studied Mg/Co multilayer is analysed by using incident photon of monochromatic energies across the Co $L_{2,3}$ absorption edge and measuring the intensity of the Co Lαβ emission. Despite large dispersive effects preventing the maxima of the electric field to reach the interfaces of the stack, it has been possible to

observe the dichroic signal in the angular distribution of the Co emission intensity, *i.e.* in the so-called x-ray standing wave curve.

INTRODUCTION

The x-ray standing waves (XSW) technique consists in measuring the intensity of a secondary emission (photoelectrons, Auger electrons or fluorescence photons) as a function of the glancing angle of the incident x-ray beam on the sample surface [1, 2]. This is done with a sample presenting a periodic structure, a crystal or a multilayer, and under the Bragg condition, *i.e.* when the glancing angle is varying around the Bragg angle set by the incident photon of a given energy and the period of the structure. Owing to the strong standing wave developing into the sample in this condition, a depth selectivity of the excitations and ionizations can be obtained [3–7]. This makes the XSW technique particularly useful for the study of periodic structures and their interfaces.

Following the pioneering theoretical study by Strange *et al.* [8] and experimental work by Hague *et al.* [9], it is now well established that the x-ray fluorescence emitted by magnetic materials presents an x-ray magnetic circular dichroism (XMCD). Consequently, it can be conjectured that the fluorescence (that is secondary x-ray emission generated by a primary x-ray source) should present a XMCD signal modulated by standing waves in periodic magnetic multilayers. In the present study, we give an experimental proof of this phenomenon.

Until this present work, XMCD has been frequently exploited in conjunction with multilayer systems through resonant scattering (that is in the vicinity of an absorption edge) in transmission or reflection mode to deduce optical constants [10], magnetic moments [11] or for quantitative polarization analysis [12] to be non-exhaustive [13, 14]. XMCD was extensively used in SW regime detecting the photoelectron current in order to analyze the magnetic properties of buried interfaces [15, 16]. But XMCD in x-ray emission (XE) and in the SW regime, referred hereafter as XSW-XE-XMCD has never been reported to our knowledge.

To perform this study, we have chosen to use the Co/Mg multilayer system that has been widely investigated and well characterized by means of a large variety of methods [6, 17, 18]. It has been shown that the Co/Mg interfaces are rather abrupt with no significant interdiffusion. It is the purpose of this paper to establish the validity and to evidence the interest of the XSW-XE-XMCD. The idea is to combine the depth selectivity of the XSW technique, which has been successfully employed to determine the interfaces of Bragg

multilayers [6] to both the chemical and magnetic selectivity of XE-XMCD in order to achieve a sub-nanometer chemically selective characterization of a magnetic profile. Indeed x-ray emission spectroscopy gives local information since it is a core level spectroscopy. It has also the advantage over Auger or photoelectron spectroscopies to probe the bulk properties. In addition, XE-XMCD provides information about the spin-resolved density of occupied states. Let us note that x-ray absorption XA-MCD is not compatible with the XSW technique since in the absorption mode the incident energy is varied while the standard XSW method requires a fixed energy. Let us mention that an important feature of emission spectroscopy is that owing to detection of photons and not of charged particles, strong magnetic fields can be applied to the sample without risk of measurement artifacts.

SIMULATIONS

The simulation model is presented in [19] and we only recall here its main characteristics. The intensity of the characteristic emission is proportional to the quantity $C(z)\,|E_{ex}(i,z)|^2\,|E_{fluo}(d,z)|^2$, where $C(z)$ is the concentration of the emitting element at a depth z under the surface of the multilayer, $|E_{ex}(i,z)|^2$ the intensity of the exciting electric field at a depth z and under a given glancing incidence angle i, and $|E_{fluo}(d,z)|^2$ the fluorescence intensity arriving at the detector under a detection angle d from a source located at depth z. The depth distribution of the incident electric field is calculated using the recurrent formalism widespread to evaluate the optical properties of a stack from the optical constants and thicknesses of its various layers [20, 21]. The emitted intensity is calculated by applying the reciprocity theorem. Owing to the large distance between the detector and the source with respect to the layer thickness, E_{fluo} is calculated by using the same formalism as the one used to calculate E_{ex}, assuming a fictive source located at infinity in the detection direction.

To emphasize the potential of the proposed methodology, we make XSW-XE-XMCD simulations for stacks presenting different kinds of defects. For these simulations, the optical constant of cobalt is taken from the literature [22], owing to its fine structure in the vicinity of the Co L_3 ($2p_{3/2}$) and L_2 ($2p_{1/2}$) edges and is given for left and right helicities (labelled “L” and “R” respectively) of the incident radiation. We consider three stacks having the same period but different structural and magnetic characteristics at the interfaces between the constituent layers, as shown in Fig. 1(a). The three stacks are the following.

1) Structure without interface defects:
B_4C (4 nm) / [Co (2.60 nm) / Mg (5.41 nm)]x30 / Si substrate;

As suggested from previous works [6], this structure is expected to best represent the multilayer we have measured in our experiment;

2) Addition of Co dead (non-magnetic, noted Co_DL) layers being thick of two atomic planes at all the interfaces; the optical constant of the dead layer is the average of the Co optical constants for left and right helicities [22]:

B_4C (4 nm) / [Co_DL (0.44 nm) / Co (1.72 nm) / Co_DL (0.44 nm) / Mg (5.41 nm)]x30 / Si substrate;

3) Addition of MgCo interphases (index calculated from CXRO [23] with a density of 6 g/cm3, same for R and L polarizations) having 0.5 nm thickness at all interfaces (0.25 nm in Mg and Co layers):

B_4C (4 nm) / [CoMg (0.5 nm) / Co (2.10 nm) / CoMg (0.5 nm) / Mg (4.91 nm)]x30 / Si substrate.

For each polarization, the XSW curve, *i.e.* the angular distribution of the intensity of the Co Lα characteristic emission is calculated when the incident photon energy is set just above the Co L3 edge, where absorption is maximum. Then the XSW-XE-XMCD curve is obtained by calculating the dichroic signal, *i.e.* making the difference between the XSW curve obtained with R and L polarizations respectively and then normalizing with respect to the sum of these two XSW curves. They are labeled (R–L)/(R+L) and shown in Figure 1(b) for the three considered stacks. First, it can be seen in the vicinity of the Bragg angle that a strong modulation of the dichroic signal exists. Then, depending on the kind of defect present at the interfaces of the stack, the maximum is shifted either to low (interphase formation) or high (dead layer) angles with respect to the stack without interface defect. This shifts are small, less than 0.1°, but should be observed in an optimized experiment. Finally, let us also note that the shape, width and background of these curves also depend on the kind of defects present in the stack.

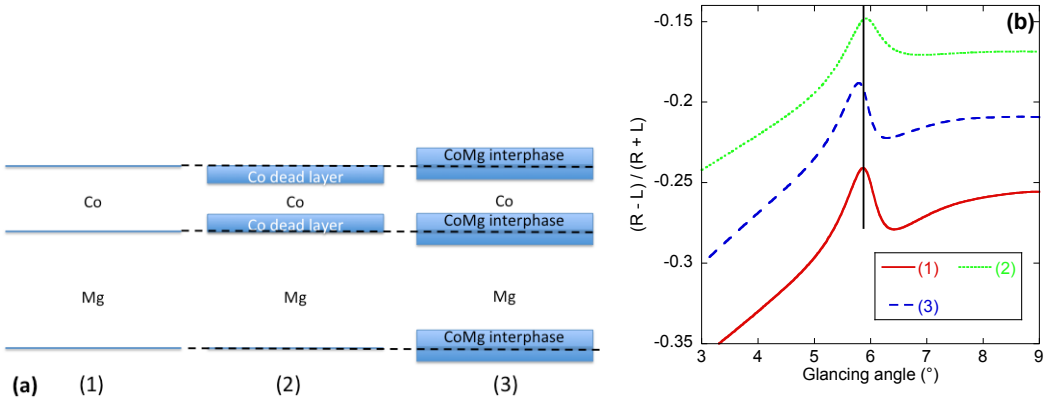

Figure 1: (a) Scheme of one period of the considered Co/Mg multilayer: (1) without interface defects; (2) with the presence Co dead layers at the interfaces; (3) with CoMg interphases at

the interfaces. (b) XSW-XE-XMCD simulated curves of the Co Lα characteristic emission obtained with stacks (1) – (3). The vertical bar indicates the position of the Bragg angle.

We show in Figure 2 the real and imaginary parts of the cobalt index extracted from Ref. [22] as a function of the energy of the incident photons in the Co $L_{2,3}$ range (~ 770 - 800 eV) and of the helicity of the radiation. The anomalous behaviour of the optical index is clearly seen in the vicinity of the cobalt edges. However, let us note that the optical indices being sensitive the chemical state of the cobalt atoms, it could be that there is still a large difference between the indices of the Co layers of our sample and the ones of Ref. [22]. Thus results of the simulations should be used with caution. For the other elements present in the multilayer, indices from the databases, such as CXRO [23], can be used as they present no absorption edge in the Co L range. Finally, let us note that the CXRO database does not reproduce correctly the optical constant of cobalt, see Figure 2, as at Co L_3 only an absorption edge is present rather than a peak and the amplitude of the real part is underestimated, and no feature exists at the Co L_2 edge.

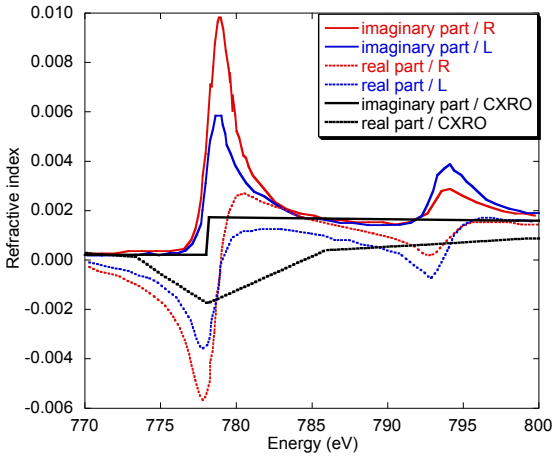

Figure 2: Real and imaginary parts of the refraction index of cobalt in the $L_{2,3}$ range extracted from Ref. [22], for L and R polarized radiations and comparison with the values of the CXRO database [23].

EXPERIMENTAL DETAILS

The sample was prepared by magnetron sputtering and had the following designed structure: vacuum / B_4C (3.0 nm) / [Co (2.6 nm) / Mg (5.2 nm)]x30 / Si substrate. The boron carbide capping layer is to prevent the oxidation of the stack. From x-ray reflectivity measurements at 8.05 keV performed just after the preparation of the sample, the actual thicknesses of the Co and Mg layers are 2.6 and 5.4 nm respectively.

The measurements were performed at the BESSY-II synchrotron facility using the reflectometer at the Optics beamline [24, 25]. The beamline is equipped with a plane-grating monochromator in collimated light (c-PGM) and can be tuned to linearly (in-plane) or elliptically polarised (off-plane) bending magnet radiation. The multilayer was first magnetized outside the experimental chamber and then measurements were taken for reversed R and L helicities of the incident radiation. Let us note that:

- magnetization was applied with a permanent magnet so that the direction of magnetization is in the plane of the sample and parallel to the scattering plane;
- changing the polarization leads to a strong variation of the incoming intensity and to a shift of the photon energy requiring a careful calibration and normalization procedure.

We measured Co L emission spectrum of the magnetized Mg/Co periodic multilayer mirror. An incident monochromatic x-ray beam was used, with both left and right circular polarizations. Some measurements have also been done with linear polarization. The characteristic emission of the cobalt atoms generated upon the x-ray irradiation, *i.e.* the fluorescence, was measured with a silicon drift detector (SDD, from Ketek). The SDD was installed a few centimeters above the sample and perpendicular to the incident x-ray beam as depicted in Figure 3. Its spectral resolution is around 70 eV in the Co L range.

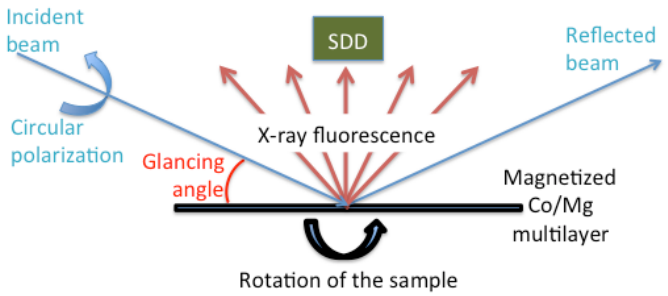

Fig. 3: Scheme of the instrumental setup and geometry of the experiment. The sample is rotated in an angular range around the Bragg angle defined by the period of the multilayer and the wavelength of the incident radiation.

All emission spectra were obtained with at least 20000 counts at their maximum, in order to obtain a statistical uncertainty lower than 1%. They were corrected for the dead time of the detector, which was about 1%. By rotating the sample, the glancing angle of the incident beam on the sample surface was changed. In this way it is possible to shift along the depth direction the x-ray standing wave field inside the multilayer to obtain a variation of the fluorescence intensity. Such an angular variation is hereafter called a XSW curve. The precision of the incidence angle is 0.02°, and the positioning accuracy of the sample surface is

approximately 0.02 mm. The focal size is 0.36 x 0.2 mm, and the energy resolution was set to 500 meV.

In Figure 4 the x-ray absorption spectra in the Co $L_{2,3}$ range clearly evidence the dependence of the absorbed intensity on the helicity of the incident radiation. These spectra are obtained at a glancing angle of 20°, in the total electron yield mode monitored from the measurement of the drain current of the sample. All spectra are normalized with respect to both their acquisition time and the intensity of the incoming beam. The absorption in the Co L_3 range is larger with R polarization while the absorption in the Co L_2 range is larger with L polarization. Measurement in linear polarization gives an intermediate behaviour. The TEY measurements validate the normalization process and so the same normalization procedure was applied on emission spectra. Moreover, they confirm that the magnetization of the sample was applied in the correct direction but show that the amplitude of the dichroic effect is not so strong as expected [22], probably due to a too weak magnetization that did not reach its saturation value.

To generate the fluorescence of the cobalt atoms, three different incident photon energies were chosen from the absorption spectrum: at the maximum of the L_3 absorption, at the maximum of the L_2 absorption and about 15-20 eV above the L_2 edge.

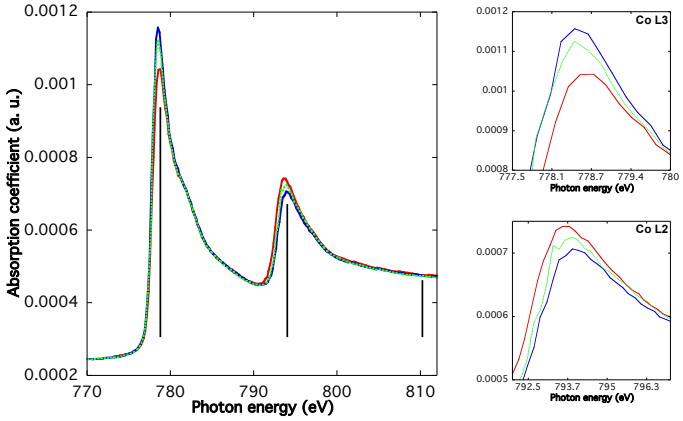

Fig. 4: Dichroism of the Co $L_{2,3}$ absorption spectrum of the magnetized Co/Mg multilayer measured with L (red line) and R (blue line) circularly polarized radiations. The three vertical bars show the three incident photon energies chosen to perform the fluorescence measurements. The insets show an enlargement of the regions of the Co L_3 and L_2 maxima. For comparison, the measurement obtained with linear radiation (green line) is also shown.

RESULTS AND DISCUSSION

An example of the measured and decomposed fluorescence spectra is shown in Figure 5. In the main peak of the experimental spectrum are present the unresolved Co Lα (3d – $2p_{3/2}$ electron transition) and Lβ (3d – $2p_{1/2}$ transition) characteristic emissions [26]. Indeed, owing to the spectral resolution of the SDD, the energy difference between the Lα and Lβ emissions represents around two channels. The shoulder toward the low photon energies (small channel numbers) is mainly caused by incomplete charge collection with a small contribution of the Co Ll (3s – $2p_{3/2}$ transition) and Lη (3s – $2p_{1/2}$ transition) emissions [26]. Let us note that the intensity of this structure strongly depends on the count rate. Since its tail is of significant intensity in the range of the Co Lαβ emission, this introduces an uncertainty on the intensity values obtained from the fitting process.

To extract the contribution of Co Lαβ emissions alone, we first fit the sum of all the obtained spectra with three Gaussians, regardless the energy or polarization of the incident beam. Figure 5 also shows the fitting result with a main contribution due to Co Lαβ emissions (shadowed area) as well as the secondary peak in the lower channel part. A tiny contribution located at higher channel (around 120) is also found. It should be the Co $L\beta_{3,4}$ (870 eV, $3d_{3/2}$ – $2s_{1/2}$ transition [26]) emission. A linear background is subtracted. Then in the following, to fit each spectrum obtained under a given polarization and a given angle, both the position and width of these three Gaussian functions are fixed and only their intensity is fitted. Finally, for a given polarization, the intensity of the Co Lαβ component is extracted for all angles to obtain the corresponding XSW curve.

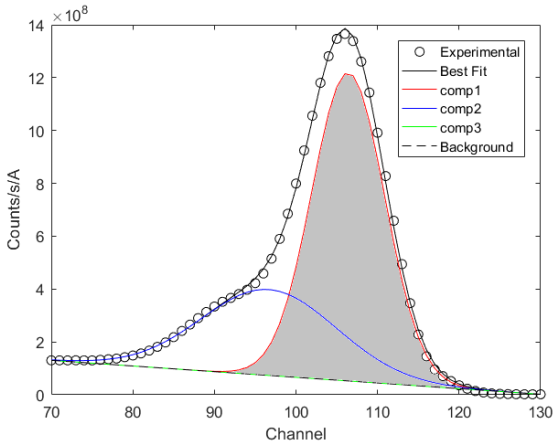

Fig. 5: Fluorescence spectrum and extraction of the different components from the sum of all fluorescence spectra. In the shadowed area are the Co Lαβ emissions, whose intensity is taken into account to establish the XSW curves.

In Figure 6 are presented the XSW curves of the extracted Co Lαβ intensities for the three considered incident energies (at the maximum of the L_3 (a) and L_2 (b) absorption and above the L_2 edge (c)), with either left or right circularly polarized lights. The 3 – 9° angular range spans the range first diffraction order of the multilayer. The value of the Bragg angle is determined by x-ray reflectivity using the same incident photon energy as for the fluorescence measurement. The error bars represent the counting statistics uncertainty with three standard deviations. However, the observed fluctuations are larger and probably come from the fitting process. When measurements are done at the L_3 maximum of the absorption, curves are almost parallel but the L one is about 10% more intense than the R one. At the L_2 maximum, curves are quite parallel but the L one is about 5% more intense than the R one. These intensity differences are due to the dichroism in the emission of the cobalt atoms. Above the L_2 edge, curves are almost superimposed, within the experimental uncertainty, except toward the lower angles.

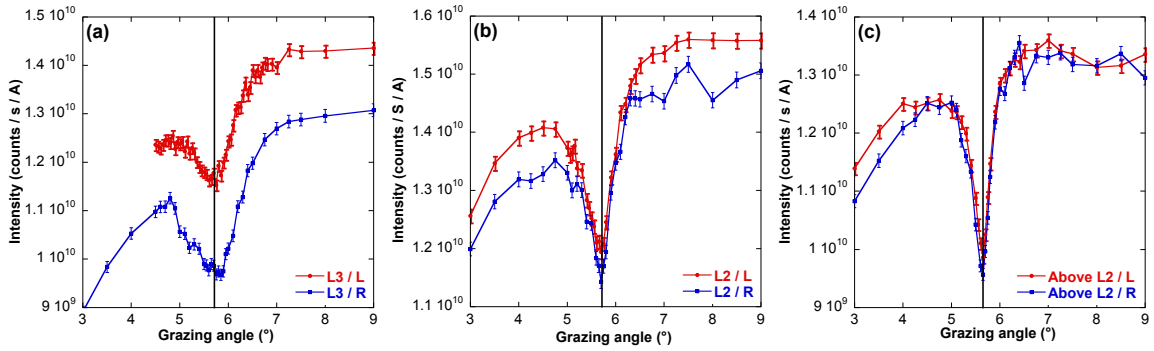

Fig. 6: XSW curves of Co Lαβ intensity from the magnetized Mg/Co multilayer measured with three different incident photon energies: at the L_3 maximum (a), at the L_2 maximum (b) and above the L_2 edge (c) and with two opposite helicities (L, red line; R blue line). The vertical bar marks the position of the Bragg angle. The error bars represent the counting statistics.

As we know from our previous studies that the interfaces between the Mg and Co layers are sharp [17, 18], we expect that Co atoms are in their standard magnetic state (as in bulk Co) in the whole layer and that only the Co interfacial atoms in contact with the Mg atoms change their magnetic property. Indeed, the magnetic moments and interactions at an interface (or a surface) can be different from the bulk, both for extrinsic (roughness, interdiffusion, strain) and intrinsic (different magnetic and chemical environments) effects experienced by the interfacial atoms [27–29]. Consequently, at the angles corresponding to the positions of the

maxima (nodes) of the electric field at the interfaces between the Mg and Co layers, expect a modification of the dichroism.

From Figure 6 we calculate the dichroic XSW-XE-XMCD curves calculated as (L-R)/(L+R) presented in Figure 7 at the L_3 and L_2 maxima and above the L_2 edge. We see when the incident energy is on the L_3 edge (Fig. 7(a)) and on a particular angular range from 5 to 6.5° that the dichroic effect has significantly changed. However, the change spans a large angular range and not the narrow one expected when crossing a sharp interface. The simulation presented in Figure 1(b) can only reproduce the main feature of the experimental curve at the Co L_3 edge, a wide peak whose maximum is located around 5.8°. The variations at the L_2 edge (Fig. 7(b)) are in the opposite of the ones at the L_3 edge, with a minimum around 5.8°, but are at the limit of the uncertainty. Above L_2 (Fig. 7(c)) we can consider that there is no dichroism within the experimental uncertainty.

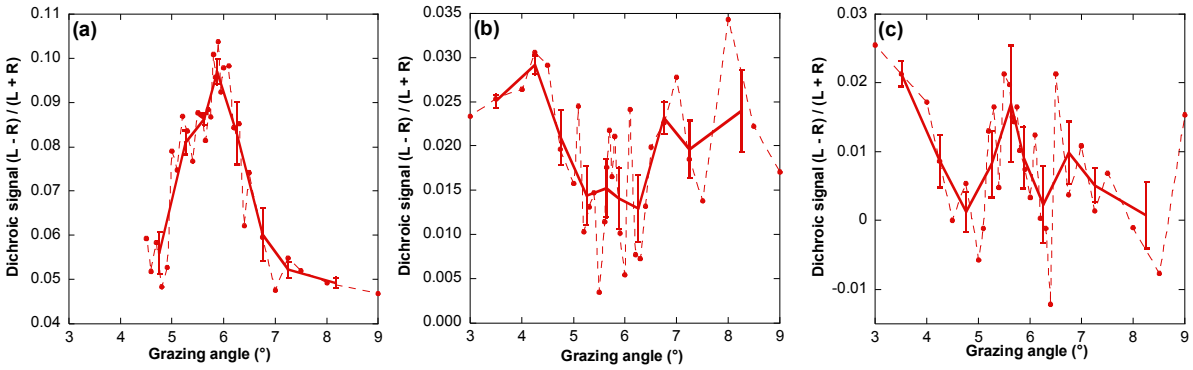

Fig. 7: XE-XSW-XMCD curves, dots and thin dashed line, *i.e.* dichroism of the XSW curves of the Co Lαβ intensity from the Co/Mg magnetized multilayer, at the three considered incident photon energies: at the L_3 maximum (a), at the L_2 maximum (b) and above the L_2 edge (c). The thick line is obtained from the original experimental points through a decimation procedure of neighbouring values. The error bars represent the standard deviation of the averaged neighbouring values.

The simulation of the depth distribution of the intensity of the electric field in the perfect Mg/Co multilayer (without interface defect) is presented in Figure 8(a), with the incident photon energy set at the Co L_3 absorption maximum and under the Bragg condition (grazing angle set to 5.6°). Further simulations in the 4 – 7° angular range, see an example in Figure 8(b) with the grazing angle set at -0.5° from the Bragg condition, show that the maximum of the electric field always stands in the Mg layers whatever the helicity, resulting that on XSW curve of Co Lα emission (see Fig. 6) we observe only “valley” and no “peak” (generally the observed fluorescence XSW feature is a valley followed by a peak or a peak

followed by a valley). For the incident photon energy at the Co L_2 edge or above, the maximum of the electric field is always varying within the Mg layer while rotating the grazing angle around the corresponding Bragg angle. Let us note that with the CXRO values of the optical indices, it would be possible to put the maxima of the electric field at the Co-on-Mg interfaces. If it was possible to set the maxima electric field at interfaces, where a reduced magnetic moment for the interfacial Co atoms is expected due to a reduced number of exchange interactions with first neighbours, then the dichroism should decrease and we should observe a dichroic signal going toward zero. Let us note that in the case of sharp interfaces an alignment of the magnetic moments can occur and, in this case, would reinforce the dichroism.

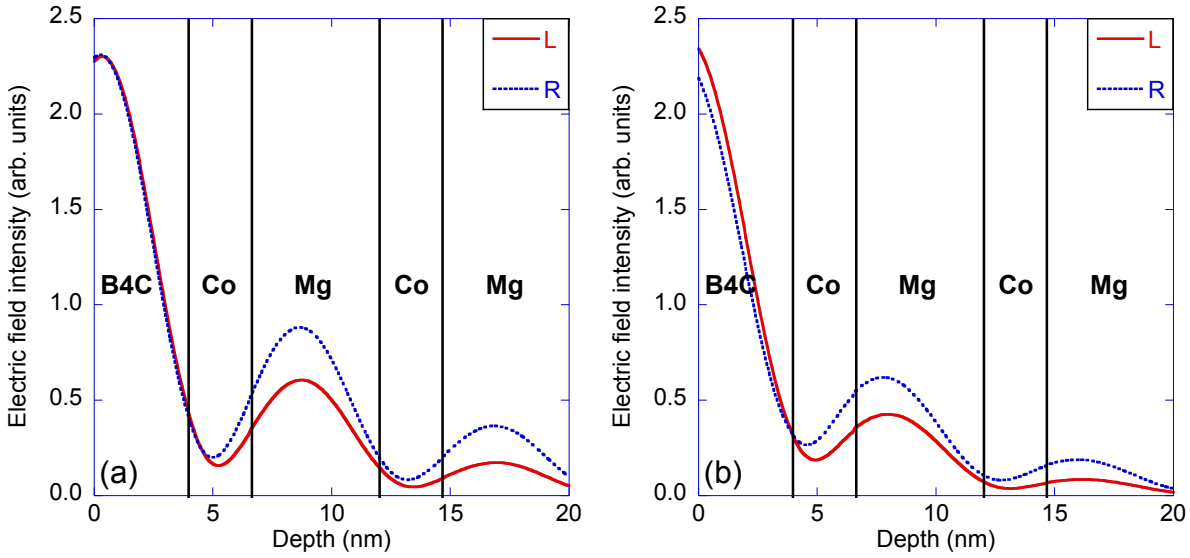

Fig. 8: Simulation of the depth distribution of the intensity of the electric field within the Mg/Co multilayer (a) under the Bragg condition, grazing angle set to 5.6°, and (b) at 5.1°, with the incident photon energy set at the Co L_3 maximum and using L (solid curve) and R (dotted curve) helicities of the radiation. Only the region of the B_4C capping layer and the two first Co/Mg periods is depicted.

The impossibility to put the maxima of the electric field at the interfaces comes from the large dispersive effect occurring taking place in the Co L range. We noted that this also induced a behaviour of the reflectivity curves quite different from the Bragg law. We show in Figure 9 the angular position, measured on reflectivity curves, of the first diffraction order Bragg peak as a function of the incident energy of the photons. For comparison, the position of the Bragg peak, calculated applying the Bragg law for a structure of period 7.8 nm is also plotted. This illustrates that the measured Bragg angle values deviate from the Bragg law in the region of the L_3 and L_2 edges and demonstrates the existence of anomalies owing to the presence of the Co L_3 and L_2 edges.

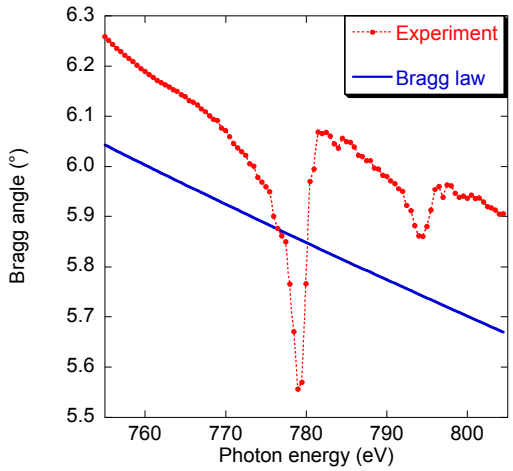

Fig. 9: Angular position of the Bragg peak as a function of the energy of the incoming photons in the Co L range (dots), compared to the Bragg law calculated with a structure of 7.8 nm period (solid line).

CONCLUSION

Owing to the complexity of the phenomena taking place at the interfaces of magnetic hetero-structures, such as electronic, orbital, and structural effects, spin transport, spin texture [27], it becomes critically important to progress towards a better understanding in the magnetic properties and the mechanism of formation of interfaces of magnetic thin film structures. As a consequence, it is extremely necessary to develop new approaches to the study such systems in order to develop future performing devices.

In this context, we presented a first test to determine the magnetic state of cobalt atoms in Co/Mg hetero-structures by using an original combination of dichroism of fluorescence (XE-XMCD) and x-ray standing waves (XSW). The present work must be considered as a test of feasibility. From the experimental point of view the operating conditions were not optimal since the sample was not fully magnetized and so the dichroic effect was limited. The counting statistics has also to be improved in order to reduce the uncertainty of the measurements. Moreover, when taking into account realistic optical indices, it is not possible to put the maxima of the electric field at the Co-on-Mg or Mg-on-Co interfaces, so that it was not possible to obtain the Co Lαβ emission selectively excited at these locations. As the interfaces in the Mg/Co system are sharp and present no interdiffusion, limited information about the physicochemical state of an interdiffused layer can be determined from our experiments with this sample. Nevertheless it turns out from this work that XE-XMCD in XSW regime can be observed and should provide interesting data about buried interface in terms of chemical and

magnetic profile as suggested by our simulations and by previous works using a standing wave generator to provide in depth-selectivity to study magnetic buried interfaces [15, 16, 30].

To improve the next experiments, the perspectives are: first, use a new generation SDD in order to get rid of, or at least minimize its sensitivity to the count rate, the peak due incomplete charge collection and to be able to work with higher counting rates to minimize the acquisition time; use a crystal spectrometer to resolve Co Lα and Lβ emissions and do not observe a dichroic effect which is the mean of the dichroic effect occurring for each of these emissions and that can have opposite behaviours. Moreover, it has been recently demonstrated a large dichroism in the Fe Kα emission on a iron single crystal [31]. Thus, it could be envisaged to apply the proposed methodology to the study of single crystals provided the wavelength of the incident radiation is consistent with the inter-reticular distance, *i.e.* if working in the hard x-ray range.

Acknowledgments

Dr. R. Delaunay from LCPMR is thanked for is help regarding the magnetization of the sample. Dr. Y. Ménesguen from CEA-LNHB is thanked for his advices regarding the SDD. A.V. is thankful to Regione Lazio and CRUL for financial support.

REFERENCES

1. D. K. G. de Boer, *Phys. Rev. B* 44, 498 (1991).

2. J. Zegenhagen and A. Kazimirov, *The X-Ray Standing Wave Technique: Principles and Applications*, World Scientific (2013).

3. M. Watanabe, T. Ejima, N. Miyata, T. Imazono, and M. Yanagihara, *Nucl. Sci. Tech.* 17, 257 (2006).

4. S.-H. Yang, A. X. Gray, A. M. Kaiser, B. S. Mun, B. C. Sell, J. B. Kortright, and C. S. Fadley, *J. Appl. Phys.* 113, 073513 (2013).

5. A. X. Gray, *J. Electron Spectrosc. Relat. Phenom.* 195, 399 (2014).

6. Y. Tu, Y. Yuan, K. Le Guen, J.-M. André, J. Zhu, Z. Wang, F. Bridou, A. Giglia, and P. Jonnard, *J. Synchrotron Radiat.* 22, 1419 (2015).

7. M. Wu, C. Burcklen, J.-M. André, K. L. Guen, A. Giglia, K. Koshmak, S. Nannarone,

F. Bridou, E. Meltchakov, S. de Rossi, F. Deltte, and P. Jonnard, *Opt. Eng.* 56, 117101 (2017).

8. P. Strange, P. J. Durham, and B. L. Gyorffy, *Phys. Rev. Lett.* 67, 3590 (1991).

9. C. F. Hague, J.-M. Mariot, P. Strange, P. J. Durham, and B. L. Gyorffy, *Phys. Rev. B* 48, 3560 (1993).

10. M. Sacchi, C. F. Hague, L. Pasquali, A. Mirone, J.-M. Mariot, P. Isberg, E. M. Gullikson, and J. H. Underwood, *Phys. Rev. Lett.* 81, 1521 (1998).

11. M. Sacchi, A. Mirone, C. F. Hague, J.-M. Mariot, L. Pasquali, P. Isberg, E. M. Gullikson, and J. H. Underwood, *Phys. Rev. B* 60, R12569 (1999).

12. E. Meltchakov, H.-C. Mertins, W. Jark, and F. Schäfers, *Nucl. Instrum. Methods Phys. Res. Sect. Accel. Spectrometers Detect. Assoc. Equip.* 467–468, 1411 (2001).

13. J. Fink, E. Schierle, E. Weschke, and J. Geck, *Rep. Prog. Phys.* 76, 056502 (2013).

14. S. Macke and E. Goering, *J. Phys. Condens. Matter* 26, 363201 (2014).

15. S.-K. Kim and J. B. Kortright, *Phys. Rev. Lett.* 86, 1347 (2001).

16. S.-H. Yang, B. S. Mun, N. Mannella, S.-K. Kim, J. B. Kortright, J. Underwood, F. Salmassi, E. Arenholz, A. Young, Z. Hussain, M. A. V. Hove, and C. S. Fadley, *J. Phys. Condens. Matter* 14, L407 (2002).

17. K. Le Guen, M.-H. Hu, J.-M. André, P. Jonnard, S. K. Zhou, H. C. Li, J. T. Zhu, Z. S. Wang, and C. Meny, *J. Phys. Chem. C* 114, 6484 (2010).

18. M.-H. Hu, K. Le Guen, J.-M. André, S. K. Zhou, H. C. Li, J. T. Zhu, Z. S. Wang, C. Meny, N. Mahne, A. Giglia, S. Nannarone, I. Estève, M. Walls, and P. Jonnard, *Appl. Phys. A* 106, 737 (2012).

19. P. Jonnard, Y.-Y. Yuan, K. Le Guen, J.-M. André, J.-T. Zhu, Z.-S. Wang, and F. Bridou, *J. Phys. B At. Mol. Opt. Phys.* 47, 165601 (2014).

20. P. H. Berning, Theory and calculations of optical thin films, in *Physics of Thin Films*, NewYork, London, G. Hass (1963), pp. 69–122.

21. M. J. Bedzyk and J. A. Libera, X-ray standing wave in multilayers, in *The X-Ray Standing Wave Technique*, World Scientific (2013), pp. 122–131.

22. D. Zhu, PhD Thesis, Standford University, *Lensless Holography Methods for Soft X-ray Resonant Coherent Imaging*, (2010).

23. CXRO X-Ray Interactions With Matter at <http://henke.lbl.gov/optical_constants/>

24. F. Schäfers, P. Bischoff, F. Eggenstein, A. Erko, A. Gaupp, S. Künstner, M. Mast, J.-S. Schmidt, F. Senf, F. Siewert, A. Sokolov, and T. Zeschke, *J. Synchrotron Radiat.* 23, 67 (2016).

25. A. Sokolov, P. Bischoff, F. Eggenstein, A. Erko, A. Gaupp, S. Künstner, M. Mast, J.-S. Schmidt, F. Senf, F. Siewert, T. Zeschke, and F. Schäfers, *Rev. Sci. Instrum.* 87, 052005 (2016).

26. P. Jonnard and C. Bonnelle, *X-Ray Spectrom.* 40, 12 (2011).

27. F. Hellman, A. Hoffmann, Y. Tserkovnyak, G. S. D. Beach, E. E. Fullerton, C. Leighton, A. H. MacDonald, D. C. Ralph, D. A. Arena, H. A. Dürr, P. Fischer, J. Grollier, J. P. Heremans, T. Jungwirth, A. V. Kimel, B. Koopmans, I. N. Krivorotov, S. J. May, A. K. Petford-Long, J. M. Rondinelli, N. Samarth, I. K. Schuller, A. N. Slavin, M. D. Stiles, O. Tchernyshyov, A. Thiaville, and B. L. Zink, *Rev. Mod. Phys.* 89, 025006 (2017).

28. F. Huang, M. T. Kief, G. J. Mankey, and R. F. Willis, *Phys. Rev. B* 49, 3962 (1994).

29. C. M. Schneider, P. Bressler, P. Schuster, J. Kirschner, J. J. De Miguel, and R. Miranda, *Phys. Rev. Lett.* 64, 1059 (1990).

30. K. Sato, M. Sugawara, T. Jinno, M. Toyoda, T. Hatano, A. Arai, and M. Yanagihara, *J. Phys. Conf. Ser.* 83, 012012 (2007).

31. T. Inami, *Phys. Rev. Lett.* 119, 137203 (2017).